ELSEVIER

Synthetic Metals 86 (1997) 1781-1784

SYNTHETIC METALS

Photolithographic patterning of the charge-density-wave conductor $Rb_{0.30}MoO_3$

H. S. J. van der Zant, O. C. Mantel, C. P. Heij and C. Dekker

Department of Applied Physics and DIMES, Delft University of Technology, Lorentzweg 1, 2628 CJ Delft, The Netherlands

Abstract

We report on the first photolithographic patterning of a charge-density wave (CDW) film. Electrical transport measurements on 2 μm structures patterned in $Rb_{0.30}MoO_3$ films reveal the expected Peierls transition near 180 K. Nonlinear current-voltage characteristics demonstrate the sliding of CDWs. Patterned structures permit unprecedented studies of mesoscopic, phase-coherent CDW transport as well as the exploration of devices based on CDWs.

Keywords: thin films, transport measurements, charge-density waves

1. CDW conductors

Electrical conductors with a chain-like structure may exhibit a phase transition to a collective ground state with charge-density waves (CDWs) [1]. At low temperatures, the lattice of atoms is distorted and the electrons condense into a ground state with a periodic modulation of the charge density. This Peierls phase transition [2] has been observed in a variety of inorganic CDW materials such as $NbSe_3$, TaS_3 and the blue bronzes $A_{0.30}MoO_3$ with A = K, Rb, Cs [3,4].

Below a certain threshold field E_T, CDWs are pinned to impurities in the crystal and electrical transport is only due to single quasiparticles that are thermally activated above the excitation gap. Above E_T, collective transport occurs when CDWs slide along the 1D chains. This sliding of CDWs has shown remarkable phenomena such as ac current oscillations induced by a dc electric field and strongly nonlinear electrical properties. Collective CDW transport displays many similarities with transport in superconductors, with the role of current and voltage reversed. For example, a current-frequency relation exists for the collective CDW current, analogous to the ac Josephson relation between voltage and frequency in superconductors.

Most dynamic CDW properties can qualitatively be understood within the Fukuyama-Lee-Rice (FLR) model [5]. In this model, the CDW is viewed as an elastic medium that interacts with impurities. Within the FLR phase-coherence length the elastic medium is undistorted by the impurities. The coherence length is typically of the order of microns along the CDW chains and much smaller in the directions perpendicular to the chains. Finite size effects are expected to occur when sample dimensions become smaller than these phase coherence lengths. Measurements on crystals with very small cross sections ($S < 1$ μm^2) have shown an increase of E_T [6-8] and a decrease of the Peierls temperature T_P [6] with decreasing S. A controlled study of CDW dynamics on these short length scales, however, has not been performed.

2. Thin films of CDW conductors

Experiments on CDWs so far have been performed on bulk crystals. Recently, we have reported on thin-film growth of the CDW oxide $Rb_{0.30}MoO_3$ [9]. With standard lithographic techniques, (sub)micron CDW structures of arbitrary shape and well-defined dimensions can now be obtained to study phase-coherent CDW transport. A thin-film technology not only permits the study of well-defined structures, but also of completely new artificial structures. Deposition of CDW materials can be combined with deposition of either normal metals, superconductors or insulators to form multi-layers or to fabricate CDW junctions. Such mesoscopic structures open up a new line of research in the field of CDWs. The first theoretical predictions on mesoscopic CDW conductors have just appeared [10].

A thin-film technology of CDW conductors may also be of importance for applications. Thin-film devices with Josephson junctions are important in applications of superconductivity. Such devices are unexplored for CDW systems due to the absence of CDW thin films. Possible applications may use the strongly nonlinear behavior of CDW materials at low fields and the fact that CDW polarization leads to extremely high dielectric constants ranging from $> 10^8$ at low frequencies to $\sim 10^3$ at microwave frequencies. The first three-terminal CDW device has recently been fabricated [11], but integration in applications seems difficult since it was made out of a bulk crystal.

3. Thin-film growth of $Rb_{0.30}MoO_3$

We use pulsed-laser deposition for the fabrication of thin $Rb_{0.30}MoO_3$ films [9]. All films are granular with most grains oriented such that the CDW-axis (=b-axis) is par-

PII S0379-6779(96)04588-2

allel to the substrate surface. Grain size increases with increasing substrate temperature and decreasing deposition rate. Surface corrugation increases with increasing deposition temperature and is substantial (of the order of the film thickness for films grown at temperatures 440-500 °C).

On $Al_2O_3(012)$ substrates, disk-like grains of submicron sizes are formed at substrate temperatures of 375-400 °C. At higher deposition temperatures, the grains have a more elongated shape. At 440 °C these grains are about 1 μm long, but at 500 °C large elongated grains with sizes up to 100 μm have formed. Grains are randomly distributed on the substrate surface. X-ray analyses demonstrate that the *b*-axis is also randomly oriented within the surface plane.

On $SrTiO_3$ substrates, we find hetero-epitaxial growth. On $SrTiO_3(100)$, elongated grains are oriented in two perpendicular directions along the principal axes of the substrate surface lattice. The b-axis runs parallel to the long axes of these grains. Depending on the deposition rate, films grown at 375 °C have grains with sizes of 0.1 by 0.5 μm^2 to 0.3 by 1 μm^2. Films grown at 440 °C have larger grain sizes ranging from 0.2 by 1 μm^2 to 1 by 5 μm^2. By using $SrTiO_3(510)$ substrates, the majority of the grains can be oriented in one direction if they are grown at 375 °C. The submicron grains have an elongated shape and their long axis runs along the [001]-axis of the $SrTiO_3(510)$ substrate.

4. Photolithography on $Rb_{0.30}MoO_3$ thin films

Standard photolithography is done with SR1813, a positive resist sensitive to near-UV light. When spin coated at a speed of 5000 rpm, this resist is 1.3 μm thick in the middle of the samples. Since our substrates are small, typically 5 by 5 mm^2, a substantial part near the sample edges has a thicker resist layer. After applying the resist, the sample is baked at 90 °C during 30 minutes. A thick resist layer is chosen because of the large surface corrugation of our films and because the resist serves as an etch-mask for the patterning of the films. Exposures are made through a glass mask with a Karl Susz aligner. The resist is then developed in a water-based AZ-developer for 45-75 s. Dry argon ion milling is done in a home-made set-up with a Kaufmann source. During etching, the sample is water cooled. Blue bronze is typically etched at a rate of 300-450 nm per hour. This rate is about a factor 5 slower than the etch rate of evaporated gold films.

We found that it is difficult to use lift-off masks; i.e., to first apply resist and evaporate metal contacts at the places where the resist is developed. When developing the resist, large parts of the $Rb_{0.30}MoO_3$ film peel off from the substrate. Probably, the water in the developer affects the $Rb_{0.30}MoO_3$ film. Better results are obtained when using an etchmask as is illustrated in Fig. 1. The film is first covered with a metal. Resist is applied to the film-metal sandwich. Upon removal of the metal by use of dry etching, contacts are formed at those places where the resist has been developed. Subsequently, the remaining resist is removed in acetone for 5 minutes. In this way, the $Rb_{0.30}MoO_3$ film is never in contact with water. Figure 2 shows the voltage probes of a completed sample. The inner voltage probes are 2 μm apart; the outer voltage probes 26 μm apart. Current contacts (not shown) are placed 86 μm to the left and right

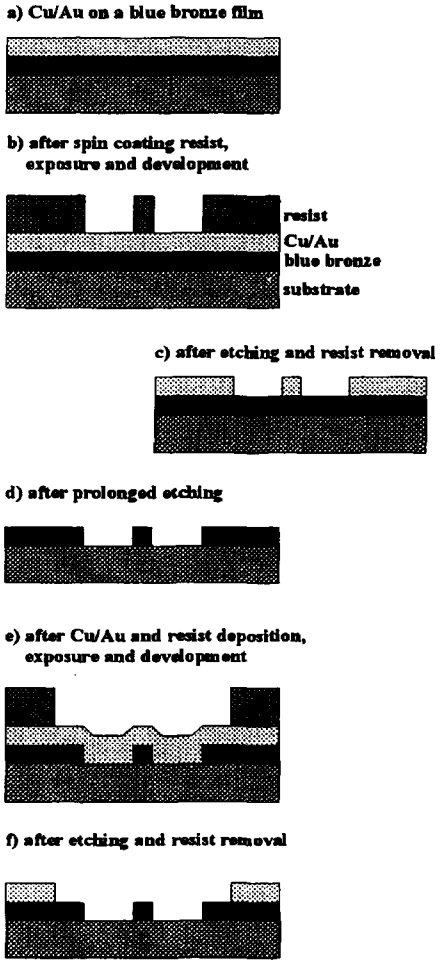

Figure 1: *Fabrication process for photolithographic patterning of (a-c) metal structures on top of a $Rb_{0.30}MoO_3$ thin film (Fig. 2) and (a,b,d-f) a $Rb_{0.30}MoO_3$ wire with metal contacts (Fig. 3).*

of the outer voltage probes.

A general problem for the processing is the bad adhesion of $Rb_{0.30}MoO_3$ to the substrate. The adhesion of the metal to the $Rb_{0.30}MoO_3$ film is generally also poor. We have tried several ways and combinations of metals to overcome this problem. In-situ laser-deposition of gold directly after the $Rb_{0.30}MoO_3$ deposition did not work since films are no longer single-phase $Rb_{0.30}MoO_3$. In-situ gold contacts can be made at room temperature, but these do not show any improvement over ex-situ e-beam evaporated gold contacts. To contact oxides, a 2-10 nm thick layer of Ti is often used. We found that the Ti reacts with $Rb_{0.30}MoO_3$. Structures fabricated with Ti do not show a Peierls transition. Our best results are obtained using a sandwich of 15-30 nm Cu covered with 150-300 nm Au. Wires can be ultrasonically bonded to this Cu/Au sandwich although adhesion is still not very good. The contact resistance between Cu and the $Rb_{0.30}MoO_3$ films is smaller than the resistance of $Rb_{0.30}MoO_3$ perpendicular to the CDW axis. (When using

top contacts, the current initially has to flow perpendicular to the CDW chains.) We can therefore only give an upper bound for this contact resistance. At room temperature this upper bound is 10 Ω per 100 by 100 μm^2.

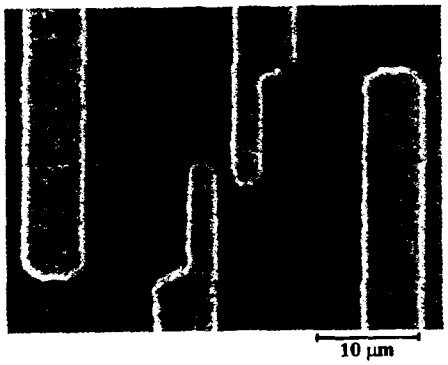

Figure 2: *An SEM picture of a fabricated copper-gold structure (sample A) on top of a $Rb_{0.30}MoO_3$ thin film showing the voltage probes which are situated in the middle of two current probes (not shown).*

A disadvantage of structures with evaporated contacts on a nonstructured film is that the current flow is not well defined. We have also fabricated 2.5 μm wide $Rb_{0.30}MoO_3$ wires such as shown in Fig. 3. The current can now be injected at both ends of the wire; voltage probes can be placed at any place in between these current contacts. The fabrication of these $Rb_{0.30}MoO_3$ wires is analogous to that outlined above. To avoid contact with water, the $Rb_{0.30}MoO_3$ films are first covered with the Cu/Au sandwich. Structures are then obtained by etching first through the Cu/Au sandwich and subsequently through the blue bronze film. Etching is stopped when the resist and then the Cu/Au underneath the resist is removed on the places where $Rb_{0.30}MoO_3$ remains. For a $Rb_{0.30}MoO_3$ film of 450 nm thick, etching of the resist takes about as much time as the etching of $Rb_{0.30}MoO_3$, so that a $Rb_{0.30}MoO_3$ structure on a cleaned substrate is obtained. In a second lithography step, the metal contacts on top of the $Rb_{0.30}MoO_3$ wire are defined using the same procedure as sketched in Fig. 1.

5. Electrical transport of patterned $Rb_{0.30}MoO_3$ structures

To date, we have not measured electrical transport through a single grain yet. We have measured over 10 films grown at different substrate temperatures and deposition rates. In this section we will present results of the two samples shown in Figs. 2 and 3. Both films have been grown at 440 °C. The scanning-electron microscopy picture of sample A is shown in Fig. 2. The 600 nm thick film has been deposited on a $SrTiO_3(100)$ substrate at 1 nm/s. SEM pictures of a higher magnification show that there are 5 grains in parallel and 2 to 3 grains in series between the 2 μm contacts. Sample B is the sample of Fig. 3 and has been grown on an $Al_2O_3(012)$ substrate at a rate of 0.15 nm/s. Its thickness is 300 nm.

Figure 4 shows the quasi-particle resistance of sample A

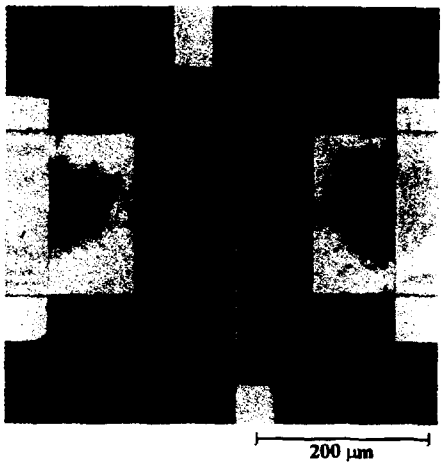

Figure 3: *A photograph of a 200 μm long and 2.5 μm wide $Rb_{0.30}MoO_3$ wire (sample B). Gold contacts at the ends are used for current injection. The voltage probes connected to the $Rb_{0.30}MoO_3$ wire are spaced 26 μm apart.*

measured as a function of temperature. The resistance is measured in the four-terminal configuration described above with standard lock-in techniques. The data clearly show the expected increase below the Peierls temperature of 180 K. The dashed line is the exponential temperature dependence with a gap according to the BCS model: $R \propto \exp[\Delta(T)/k_BT]$. The fit parameter $\Delta(0)/k_B$ is 410 K for this sample. For sample B a similar fit yields $\Delta(0)/k_B =$ 400 K. For films grown at 375 °C, we find a lower value of the zero-temperature gap whereas for films grown at higher temperature a higher value is found (460-470 K). A reduction of $\Delta(0)$ due to finite size effects may be expected but our data at this moment show too much scatter to be conclusive in this respect. More data is needed.

At room temperature, the resistivity is a few mΩcm. In a bulk crystal the resistance initially decreases with decreasing temperature. In our films, we find a slight increase of the resistance. The corresponding energy barrier in this thermally activated activation process ranges from 250 K for films grown at low temperatures to about 50-100 K for films grown at high temperatures. In Fig. 4, the energy barrier in the high-temperature region is 50 K. We ascribe the thermally activated behavior above the Peierls transition to the granular nature of our films.

The granular nature may also be responsible for the smearing of the Peierls transition itself as observed for all our samples. The inset of Fig. 4 shows the results for sample A. The variable $d(\ln(R))/dT$ is commonly used to visualize the Peierls phase transition; in crystals a clear dip in $d(\ln(R))/dT$ is observed at T_p. Our samples merely show a kink near T_p.

We have measured the current-voltage characteristics at various temperatures. Simultaneously, we have recorded the differential resistance (dV/dI) with a lock-in technique. The ac amplitude was 3 % of the full dc current-scale. For sample B, the result measured at 50 K is shown in Fig. 5. The current-voltage characteristic is clearly nonlinear. It

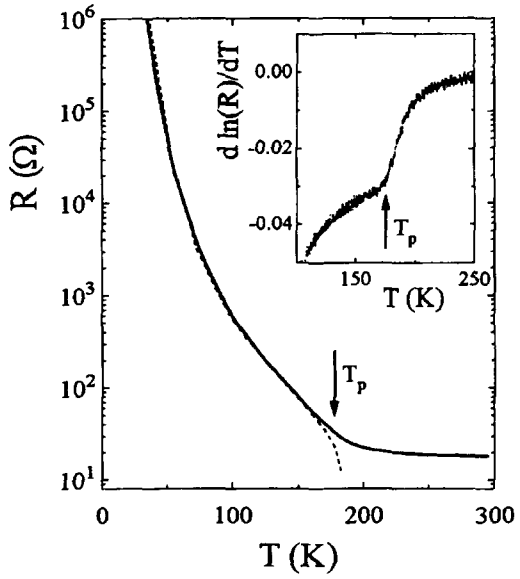

Figure 4: *The four-probe resistance across the 2 μm voltage probes of sample A vs. temperature showing the Peierls transition around 180 K. Inset: the same data plotted as d(ln(R))/dT versus T, illustrating the behavior near the Peierls transition.*

is difficult to define a threshold field since the nonlinearity appears very smoothly. In bulk crystals, a well-defined threshold field is observed if current is injected homogeneously. If we define the threshold field as illustrated in the inset of Fig. 5, its value is about 50 V/cm. For sample A, the threshold field is around 100 V/cm. These values are much higher than reported in literature. A bulk $Rb_{0.30}MoO_3$ sample with a cross section of 90 nm by 110 μm has shown a threshold field of 4 V/cm [8]. Since grains are only a few 100 nm's wide, we can not exclude that our high threshold fields are due to finite-size effects. However, it may also be that the high threshold fields are due to depinning from grain boundaries. The observation that the threshold field decreases with decreasing number of grains between voltage contacts is consistent with this picture.

6. Conclusion

We have presented the first results on patterning of a film of a CDW compound. Films consist of single-phase $Rb_{0.30}MoO_3$ and have a granular structure with grain sizes typically of the order of 1 μm. With standard photolithographic techniques, devices are fabricated containing a few grains. The quasi-particle resistance measured as a function of temperature clearly reveals the expected Peierls temperature around 180 K. Below the Peierls temperature, the resistance increases in accordance with the opening of an excitation gap. The value of the zero-temperature gap is suppressed for films with the smallest grain sizes. We clearly observe nonlinear current-voltage characteristics, indicative of the sliding of CDWs. The threshold field is higher than expected, probably due to the depinning from grain boundaries.

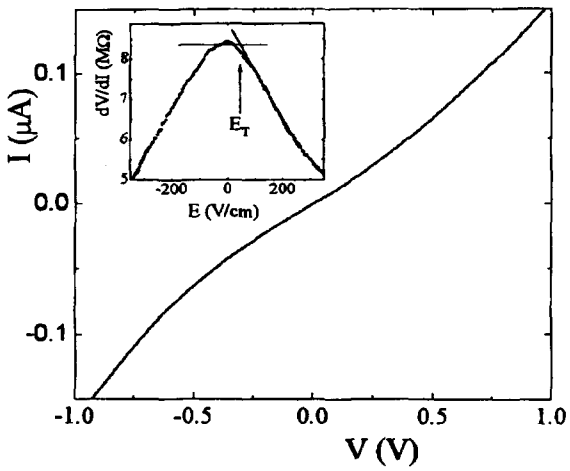

Figure 5: *(a) Two-terminal current-voltage characteristics of sample B measured at 50 K across the voltage probes. Inset: the corresponding differential resistance plotted as a function of the electric field.*

Acknowledgment

We wish to acknowledge Hans Mooij, Mark Visscher, Behzad Rejaei, and Gerrit Bauer for discussions, Leo Lander for technical assistance, Jip Steinfort for X-ray analyses, and Chresten Træholt and Henny Zandbergen for TEM work. Research was supported by the Netherlands Foundation for Fundamental Research (FOM).

References

[1] G. Grüner, *Density Waves in Solids* (Addison-Wesley Publishing Company, 1994).
[2] R. Peierls, in *Quantum Theory of Solids* (Oxford University Press, 1955) p. 108.
[3] P. Monceau, in *Electronic Properties of Quasi-One-Dimensional Metals*, edited by P. Monceau (Reidel, Dordrecht, 1985), Vol. 2.
[4] C. Schlenker, J. Dumas, C. Escribe-Filippini, and H. Guyot, in *Low-Dimensional Properties of Molybdenum Bronzes and Oxides*, edited by C. Schlenker, (Kluwer Academic Publishers, Dordrecht, 1989) 159–257.
[5] H. Fukuyama and P. A. Lee, Phys. Rev. B **17**, 535 (1978); P. A. Lee and T. M. Rice, Phys. Rev. B **19** (1979) 3970.
[6] D. V. Borodin, S.V. Zaitsev-Zotov and F. Ya. Nad', Sov. Phys. JETP **66** (1987) 793.
[7] J. McCarten, M. Mahler, T. L. Adelman and R. E. Thorne, Phys. Rev. Lett. **63** (1989) 2841.
[8] W. Xue-mei, Z. Dian-lian and Z. Yuheng, Phys. Rev. B **45** (1992) 13250.
[9] H. S. J. van der Zant et al., Appl. Phys. Lett. **68** (1996) 3823; O. C. Mantel et al., submitted to Phys. Rev. B; O. C. Mantel et al., this issue.
[10] M. I. Visscher and G. E. W. Bauer, Phys. Rev. B accepted for publication in Phys. Rev. B (June 15, 1996); B. Rejaei and G. E. W. Bauer, accepted for publication in Phys. Rev. B (August 15, 1996).
[11] T. L. Adelman, S. V. Zaitsev-Zotov and R. E. Thorne, Phys. Rev. Lett. **74** (1995) 5264.